Desalination 350 (2014) 35–43

Contents lists available at ScienceDirect

Desalination

journal homepage: www.elsevier.com/locate/desal

Desalination energy minimization using thin film nanocomposite membranes

Arun Subramani [a,*], Nikolay Voutchkov [b], Joseph G. Jacangelo [a,c]

[a] MWH, 300 North Lake Avenue, Suite 400, Pasadena, CA 91101, USA
[b] Water Globe Consulting, 200, Broad Street, Stamford, CT 06901, USA
[c] The Johns Hopkins University, Bloomberg School of Public Health, Baltimore, MD 21205, USA

HIGHLIGHTS

- SEC of TFN RO membranes were compared with TFC RO membranes.
- TFN RO membranes exhibited up to 10% savings in SEC.
- Savings in SEC for TFN RO membranes was due to lower feed pressure requirements.

ARTICLE INFO

Article history:
Received 15 May 2014
Received in revised form 4 July 2014
Accepted 6 July 2014
Available online xxxx

Keywords:
Energy recovery devices
Pump efficiency
Specific energy consumption
Boron rejection
Organic fouling

ABSTRACT

In this study, thin film nanocomposite (TFN) reverse osmosis (RO) membranes were evaluated at a demonstration-scale facility to determine the specific energy consumption (SEC) during seawater desalination. Conventional (same element type within pressure vessel) and hybrid (high and low rejection elements within pressure vessel) configurations were evaluated and compared to commercially available thin film composite (TFC) RO membranes. The specific flux at 25 °C for TFN RO membranes was 1.72 lm^{-2} h^{-1}/bar when compared to 1.48 lm^{-2} h^{-1}/bar for TFC RO membranes. Utilization of TFN RO membranes resulted in reduced feed pressure requirements when compared to TFC RO membranes, resulting in energy savings up to 10%. In order to achieve the same permeate water quality, the SEC for a 2-pass RO system with TFN RO membrane elements in the first pass was 3.24–3.45 kWh/m^3. The SEC with TFC RO membrane elements for the same conditions was 3.60 kWh/m^3. Results presented in this study show a promise for the utilization of TFN RO membranes to reduce energy consumption and minimize operational costs associated with electricity usage.

1. Introduction

Many municipalities and water suppliers are considering seawater desalination to supplement inadequate freshwater sources due to increasing water demand. By the year 2016, the global water production by desalination is projected to exceed 38 billion m^3 per year, which is twice the rate of global production for the year 2008 [1]. Desalination processes are broadly categorized as thermal or membrane-based technologies [2]. Although thermal desalination has remained the primary technology of choice in the Middle East, membrane processes, such as reverse osmosis (RO), have rapidly developed since the 1960s [3] and currently surpass thermal processes in new plant installations [2]. More than 69% of the desalination production capacity in the United States is due to the use of RO membranes [2].

Seawater desalination is a promising option for a steady supply of high-quality water from the abundantly available source of ocean water, but the conventional RO process most widely used at present is energy intensive. Costs associated with electricity are up to 50% of the total cost of desalinated water [4]. Higher energy consumption also translates to a corresponding increase in greenhouse gas (GHG) emissions [5]. Reducing energy consumption is critical for lowering the cost of desalination and addressing environmental concerns about GHG emissions from the continued use of conventional fossil fuels as the primary energy source for seawater desalination plants.

During desalination with RO membranes, seawater is pressurized against a semi-permeable membrane that allows water to pass through while rejecting salt [6]. In order to produce desalinated water, the osmotic pressure of the source seawater and the concentrate generated during the RO process need to be exceeded [7]. The feed water to the RO is pressurized using a high pressure (HP) feed pump to supply the necessary pressure to force water through the membrane to exceed the osmotic pressure and overcome differential pressure losses through the system [8]. At present, typically, an isobaric energy recovery device

* Corresponding author at: MWH Americas Inc., 618 Michillinda Avenue, Suite 200, Arcadia, CA 91007, USA. Tel.: +1 626 568 6002; fax: +1 626 568 6015.
E-mail address: Arun.Subramani@us.mwhglobal.com (A. Subramani).

http://dx.doi.org/10.1016/j.desal.2014.07.011
0011-9164/

(ERD) in combination with a booster pump is used to recover the pressure from the concentrate and to reduce the required size and energy use of the high pressure pump [8].

The energy required to desalinate seawater with RO can be expressed in terms of specific energy consumption (SEC) [8]. This is the energy required per unit output of product water from RO systems equipped with isobaric type energy recovery devices and can be calculated using the following equation [8]:

$$SEC = (E_{HP} + E_{BP} + E_{SP})/Q_P \quad (1)$$

where, SEC is the specific energy consumption (in kWh/m^3), E_{HP} is the high pressure pump-power consumed (in kW), E_{BP} is the booster pump-power consumed (in kW), E_{SP} is the supply pump-power consumed (in kW) and Q_P is the permeate flow rate expressed in m^3/h. The energy consumed by each of the RO system pumps is a function of the flow rate through the pump, pressure (total dynamic head) delivered by the pump, and the efficiencies of individual pump and motor [8]. Thus, by measuring the pressure and flow of the pumps along with the relevant motor and pump efficiencies, the SEC can be calculated.

A theoretical minimum energy is required to exceed the osmotic pressure and produce desalinated water. The energy needed for desalination using RO membranes is a function of the feed water recovery, intrinsic membrane resistance (permeability), operational flux, feed water salinity and temperature fluctuations, product water quality requirements and system configuration [4]. As the salinity of the source seawater or feed water recovery increases, the minimum energy required for desalination also increases. For example, the theoretical minimum energy for seawater desalination with 35,000 mg/L of salt and a feed water recovery of 50% is 1.06 kWh/m^3 [9]. The actual energy consumption is higher as actual plants do not operate as a reversible thermodynamic process [9]. For a similar TDS level, the lowest energy consumption reported for RO system (1st pass only) to desalinate seawater was 1.58 kWh/m^3 at a feed water recovery of 42.5% and a flux of 10.2 lm^{-2} h^{-1} (lmh) [10]. In addition, pre- and post-treatments contribute to additional energy requirements [7]. Typically, the total energy requirement for seawater desalination using RO (including pre- and post-treatments) is on the order of 3–6 kWh/m^3 [11]. Thus, reducing the feed pressure requirement during desalination is a key to reducing energy consumption.

In the recent years, several novel membrane materials have been proposed to enhance water permeability and reduce energy consumption. Some of these promising membranes are based on graphene oxide sheets [12–14], carbon nanotubes [15–18] and aquaporins [19, 20]. However, only membranes with TFN structure enhanced by zeolite nanoparticles have been commercialized to date.

Currently, TFC RO membranes are predominantly used for seawater desalination. These membranes consist of a three layer structure: a thin and dense active membrane layer (typically 100 nm in thickness), a thicker intermediate layer (approximately 40 μm) and a porous support layer [21]. A new generation of RO membrane elements, commonly referred as TFN RO membranes, has evolved based on the incorporation of nanoparticles within the active layer in order to enhance water permeability and maintain high solute rejection at the same time [22,23]. Initial development of TFN RO membranes utilized Linde type A zeolite nanoparticles within the active layer to enhance water permeability [24,25]. During commercialization of TFN membranes, alkaline earth metals, monohydrolyzed trimesoyl chloride (TMC) and other molecular additives were considered to enhance flux, maintain salt rejection and provide anti-fouling properties [26,27].

A recent study evaluated these commercially available TFN RO membranes for its performance and compared with TFC RO [28]. Results from this study indicated that the TFN RO membrane exhibited higher (twofold increase) water permeability when compared to TFC RO. However, the most important aspect of TFN RO membranes is the reduction in specific energy consumption (SEC) due to lower feed pressure requirements. The SEC of RO systems with TFN RO membranes has not been reported to date in the peer-reviewed literature. Thus, in this study, a demonstration-scale evaluation was performed to desalinate seawater using TFN RO membranes and the SEC was obtained experimentally and compared with TFC RO membrane of the same configuration and operational conditions. The specific objectives of this study were to: 1) evaluate the SEC of TFN RO systems at various operating conditions and 2) assess the performance of TFN RO membranes with respect to permeate water quality produced.

2. Materials and methods

2.1. Test site location and feed water source

Experimentation was conducted at West Basin Municipal Water District's Temporary Ocean-Water Desalination Demonstration Project site located at the L.A. Conservation Corps' SEA Lab facility in Redondo Beach, California. The feed water source was the Pacific Ocean with an open intake that utilized wedge wire screens as the first filtration step. The wedge wire screens were used to remove large pieces of debris and minimize impingement and entrainment of marine organisms. The seawater was then passed through a pretreatment process and a 2-pass RO system for desalination.

2.2. Description of treatment train

A schematic of the treatment train utilized for this study is shown in Fig. 1. The system capacity was 22.7 m^3/h and major process components of the treatment train included an Arkal microscreen disc filter, a General Electric (GE) ZeeWeed ZW1000 ultrafiltration (UF) membrane pretreatment system and a two-pass seawater RO system. After the wedge wire screens, seawater was passed through the Arkal disc filter system. The purpose of the 100 micron disc filters was to protect the UF system from damage caused by large particles, such as ocean life shell fragments. There were a total of 4 filters (2 duty and 2 standby) installed in a parallel configuration. The purpose of the UF system was to provide the required feed water quality to the RO system by removing suspended solids and maintaining a low turbidity (less than 0.1 NTU) and silt density index (SDI) (less than 2.5). The UF membrane had a nominal pore size of 0.02 μm and an outside-in geometric flow configuration. The membranes were suspended vertically in cassettes. A reverse (inside-out) flow backwash was implemented to remove foulants on the membrane surface. The backwash utilized UF filtrate water to remove any biofoulant layer. During the backwash cycle, coarse bubble aeration was also used to scour debris from the outside of the membrane surface.

The seawater RO system consisted of a two-pass system with 5 micron cartridge filters, an energy recovery device (ERD), clean-in-place (CIP) system and flush system. The 1st pass consisted of two 8-inch pressure vessels in a parallel configuration. Each pressure vessel was capable of accommodating 7 membrane elements. A Danfoss APP10.2 axial piston pump was used as the high pressure pump for the 1st pass RO system. A PX-45S ERD from Energy Recovery Inc. (ERI) was utilized for recovering the energy from the 1st pass concentrate stream. A Series 8500-2400 PX booster pump from ERI was after the ERD. A booster pump was used to boost the pressure on the high pressure portion of the system to make up the minor pressure losses that occur in the RO system, the ERD and associated piping. A portion of the 1st pass permeate (tail end elements) was sent to a 2nd pass RO system. The 2nd pass consisted of a two stage design where concentrate from the first stage was fed to the second stage and the first stage and second permeate streams were mixed together. The first stage had two pressure vessels in parallel, each containing either three or four 4-inch diameter brackish water RO elements.

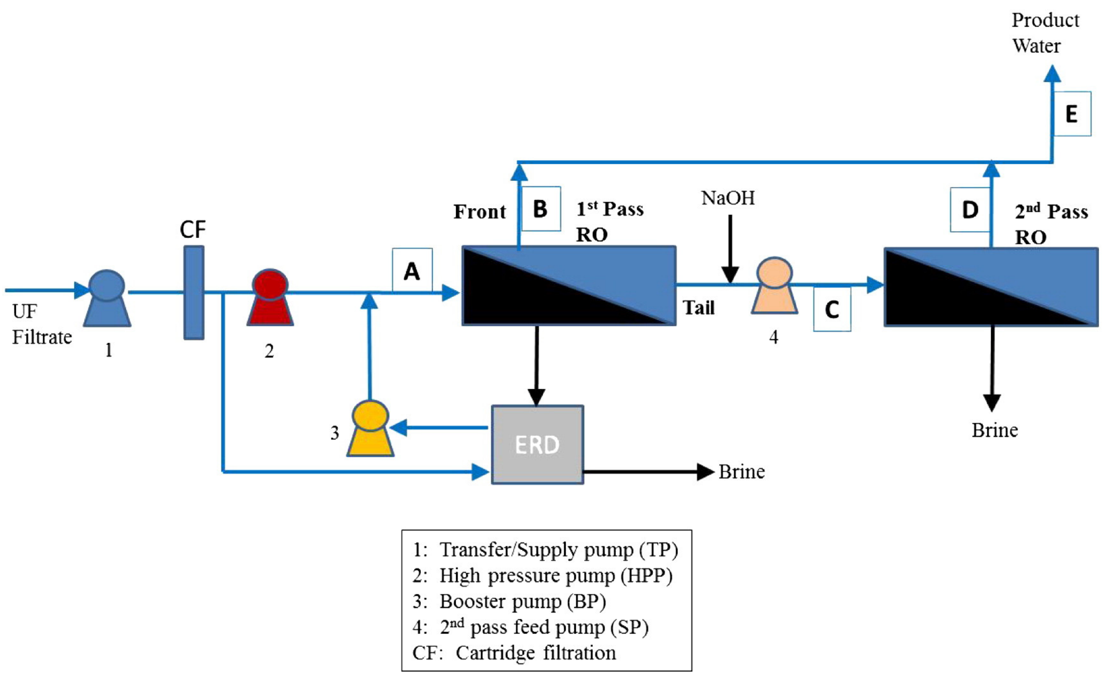

Fig. 1. Process schematic of 1st and 2nd pass RO systems utilized for evaluation of SEC.

2.3. Model membranes

The model of seawater RO membranes utilized for the study and their specifications are shown in Table 3. TFN RO membranes from NanoH$_2$O, LLC (El Segundo, California) were utilized for the study. The Qfx400ES membrane element is reported as a high permeability (52 m^3/d) nanocomposite membrane with a stabilized sodium chloride rejection of 99.8% [29]. The Qfx400R membrane element is a relatively lower permeability (34 m^3/d) nanocomposite membrane with a reported stabilized sodium chloride rejection of 99.85% [30]. The SW30ULE-400i [31] and SW30XLE-400i [32] membrane elements were obtained from DowFilmtec (Midland, Michigan) to represent TFC membranes and were used for estimation of baseline energy consumption. These membranes were selected based on similar surface area and salt rejection when compared to the TFN RO membranes. The TFN RO membrane element Qfx 400ES was compared with TFC RO membrane element SW30ULE-400i in the conventional configuration with the same element type within a pressure vessel. In the hybrid configuration, the lead (front) elements in the pressure vessel consisted of high rejection elements followed by tail (end) elements with lower rejection. For the "Hybrid 1" scenario with TFN RO membranes, the lead two elements were Qfx400R and the tail elements (last five) were Qfx400ES membranes. In the "Hybrid 2" configuration with TFN RO membranes, the lead element (first element) was a Qfx400R membrane and the tail elements (last six) were Qfx365ES membranes. Under the TFC RO membrane hybrid scenario, the lead elements (initial two) were SW30XLE-400i and the tail elements (last five) consisted of SW30ULE-400i membranes. Water quality was monitored in the 1st pass RO system to estimate the rejection properties of model membranes. Water quality parameters and analytical methods utilized are shown in Table 1. Performance of the membranes were assessed by calculating rejection, flux, temperature corrected specific flux and feed water recovery. Standard equations and correlations were utilized for estimating these performance parameters [33]. Autopsy studies were performed using scanning electron microscopy (SEM) and Fourier Transform Infrared (FTIR) spectroscopy to determine the nature and structure of the fouling layer [34].

2.4. Estimation of the SEC

The SEC was measured based on the process schematic presented in Fig. 1. The energy consumption was measured for the transfer/supply

Table 1
Summary of feed water quality parameters and analytical methods utilized in this study.

Parameter	Method
Total dissolved solids (TDS)	SM 2540C
Total organic carbon (TOC)	SM 5310C
Temperature	SM 2550B
pH	SM 4500H$^+$
Conductivity	SM 2510B
Calcium	EPA 200.7
Magnesium	EPA 200.7
Potassium	EPA 200.7
Sodium	EPA 200.7
Barium	EPA 200.8
Strontium	EPA 200.7
Bromide	EPA 300.0
Fluoride	SM 4500FC
Chloride	EPA 300.0
Sulfate	EPA 300.0
Boron	EPA 200.7

Table 2
Summary of feedwater quality from the seawater employed in study. Sampling was performed after pretreatment and prior to the 1st pass RO system.

Analyte	Units	Average	Standard deviation	Minimum	Maximum
Alkalinity	mg/L as $CaCO_3$	103	5	98	110
Boron	mg/L	4.4	0.2	4.1	5.0
Bromide	mg/L	66	3	61	71
Calcium	mg/L	384	13	370	410
Chloride	mg/L	19,065	574	18,000	20,000
Magnesium	mg/L	1252	63	1200	1400
pH	–	7.9	0.1	7.7	8.0
Potassium	mg/L	369	12	350	400
Sodium	mg/L	10,048	333	9600	11,000
Specific Conductance	μS/cm	47,226	497	46,000	48,000
Strontium	mg/L	7.2	0.2	6.9	7.9
Sulfate	mg/L	2426	68	2300	2500
TDS	mg/L	33,935	1124	32,000	37,000
TOC	mg/L	2.3	1.1	1.3	4.5

Table 3
Model membranes and manufacturer specifications.

Model	TFN RO			TFC RO	
	Qfx 400ES	Qfx 365ES	Qfx 400R	SW30ULE-400i	SW30XLE-400i
Active area, m^2	37	34	37	37	37
Permeate flow, m^3/d	52	47	34	42	34
Stabilized salt rejection, %	99.80	99.75	99.85	99.70	99.80
Boron rejection, %	89.0	89.0	93.0	89.0	91.5

pump, HP pump, ERD booster pump in the 1st pass RO system and the 2nd pass feed pump. The SEC during the study was monitored by online electrical meters that were installed for the HP pump (1st pass), the booster pump (after ERD) and the feed pump for the 2nd pass RO system. These meters directly measured the electricity draw (current in amps) from the respective motors connected to variable frequency drives. SEC based on experiments was calculated based on the current, voltage and phase for the individual motors using the following expression,

$$SEC_{EXP} = \frac{V \times I \times \sqrt{\emptyset}}{Q_P} \tag{2}$$

where, SEC_{exp} = specific energy consumption based on experimental electricity draw measurements, kWh/m^3

V voltage draw for pumps, volts
I current draw for pumps, amps
ϕ phase for motor
Q_p permeate flow rate, m^3/h.

SEC of the RO system's 1st pass was calculated based on the following expressions,

$$Power_{CALC} = \frac{Q_{HP}(P_{HP} - P_F)}{\eta_{HP}} + \frac{Q_{BP}(P_{HP} - P_{BPI})}{\eta_{BP}} \tag{3}$$

$$SEC_{CALC} = \frac{Power_{CALC}}{Q_P} \tag{4}$$

where,

$Power_{CALC}$ calculated power consumption of the 1st pass RO, kW
SEC_{CALC} calculated specific energy consumption of the 1st pass, kWh/m^3
Q_p permeate flow rate from 1st pass, m^3/h
Q_{HP} high pressure pump flow rate, m^3/h
Q_{BP} booster pump flow rate, m^3/h
P_{HP} high pressure pump outlet pressure, bar
P_F high pressure pump feed pressure, bar
P_{BPI} booster pump inlet pressure, bar
η_{HP} high pressure pump and motor efficiency, %
η_{BP} booster pump and motor efficiency, %.

Manufacturer pump curves were used to estimate the efficiency of the ERI booster pump series 8500-2400 PX at a particular flow rate and head. Efficiency of the Danfoss APP 10.2 high pressure pump was calculated using the following expression,

$$\eta HP = \frac{Power_{Required-HP\ \ Pump}}{Power_{Actual-HP\ \ Pump}} \tag{5}$$

$$Power_{Required-HP\ \ Pump} = \frac{16.7 \times Q_{HP} \times P_{HP}}{496.2} \tag{6}$$

where,

$Power_{Actual\text{-}HP\ PUMP}$ calculated power from V, I and ϕ measurements, kW
Q_{HP} flow rate of the high pressure pump, m^3/h.

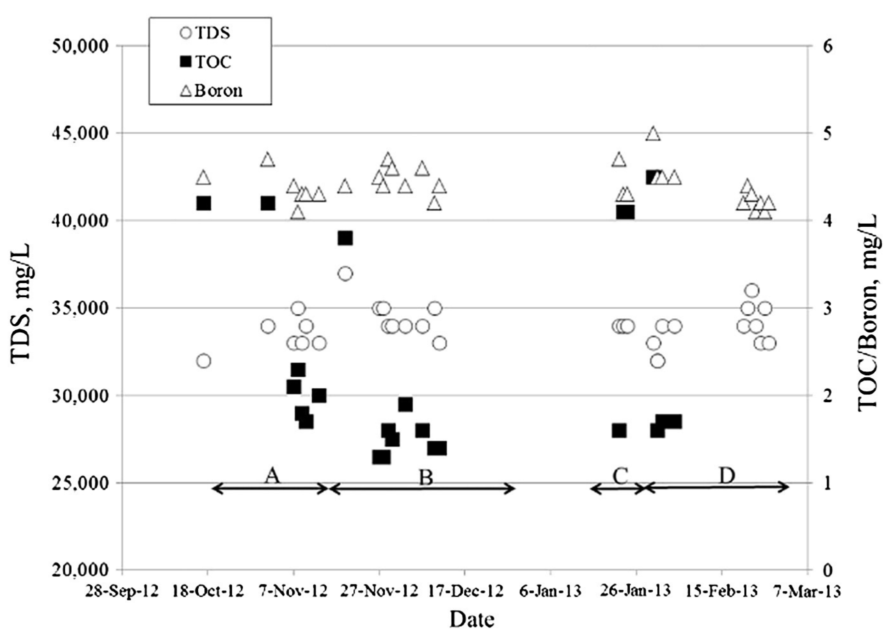

Fig. 2. Feed water quality to the RO system measured during the study. The following membrane configurations were utilized: (A) TFC RO — conventional, (B) TFC RO — hybrid, (C) TFN RO — conventional, (D) TFN RO — hybrid 1.

Table 4
Specific energy consumption for TFC RO membranes.

Membrane type/configuration	Flux	1st pass system recovery	Feed pressure	High pressure pump		ERD booster pump		SEC_{EXP}
	lmh	%	bar	Power, kW	Efficiency	Power, kW	Efficiency	kWh/m^3
TFC RO — conventional	12.0	40	49.7	13.33	77%	0.69	55%	2.30
TFC RO — conventional	12.0	45	52.7	13.66	79%	0.41	55%	2.30
TFC RO — conventional	12.0	55	61.7	14.82	85%	0.26	40%	2.45
TFC RO — conventional	15.3	45	56.3	19.34	77%	0.70	55%	2.52
TFC RO — conventional	15.3	50	61.2	20.25	80%	0.46	60%	2.60
TFC RO — conventional	15.3	55	64.8	20.92	81%	0.32	45%	2.69
TFC RO — conventional	18.7	50	64.5	26.18	78%	0.83	55%	2.80
TFC RO — hybrid	12.0	40	49.4	13.32	76%	0.70	55%	2.28
TFC RO — hybrid	12.0	45	53.9	13.99	79%	0.44	50%	2.35
TFC RO — hybrid	12.0	50	57.8	14.80	79%	0.27	50%	2.46
TFC RO — hybrid	12.0	55	63.3	15.78	82%	0.18	40%	2.62
TFC RO — hybrid	15.3	45	57.4	19.78	77%	0.84	55%	2.61
TFC RO — hybrid	15.3	50	61.6	20.18	81%	0.51	60%	2.61

3. Results and discussion

3.1. Feed water quality

Feed water quality to the RO system is provided in Table 2. The water quality did not change substantially during the study period. The feed water temperature did not vary substantially during the evaluation period, remaining between 15 and 17 °C during runs with varying operating conditions. The TDS, TOC and boron concentrations in the 1st pass RO feed are shown in Fig. 2. The boron concentration varied between 4.0 and 5.0 mg/L during the study but the concentration did not fluctuate substantially. The water quality parameter that varied substantially was the total organic carbon (TOC) concentration. During January of 2013, the TOC in the feed water increased to 4.5 mg/L, approximately twice the average concentration. The increase in TOC was potentially due to scouring of the seawater floor due to changes in wave currents during that season. The increase in TOC concentration only occurred over a short period and measured values returned to <2.0 mg/L, remaining stable during the reminder of the study.

3.2. Baseline energy consumption

Experimental SEC for the TFC RO membrane is shown in Table 4. For an operational flux of 12.0 lmh, the SEC ranged between 2.28 kWh/m^3 and 2.62 kWh/m^3. An increase in feed water recovery resulted in higher power consumption for the high pressure pump due to higher feed pressure requirement to maintain a constant flux. However, the power requirement for the ERD booster pump decreased with an increase in feed water recovery. The specific flux for the TFC RO membranes was 1.48 lmh/bar for both conventional and hybrid configurations. The efficiency of the high pressure and ERD booster pump is shown in Table 4 for various operating conditions with TFC RO membranes. The high pressure pump operated at its highest efficiency of 82% and 85% at a flux of 12.0 lmh and a 1st pass feed water recovery of 55%

Table 5
Specific energy consumption for TFN RO membranes.

Membrane type/configuration	Flux	1st pass system recovery	Feed pressure	High pressure pump		ERD booster pump		SEC_{EXP}
	lmh	%	bar	Power, kW	Efficiency	Power, kW	Efficiency	kWh/m^3
TFN RO — conventional	12.0	40	44.8	12.76	72%	0.88	55%	2.23
TFN RO — conventional	12.0	45	48.3	12.86	78%	0.53	55%	2.19
TFN RO — conventional	15.3	45	50.3	15.22	88%	1.11	55%	2.06
TFN RO — conventional	15.3	50	54.6	18.63	78%	0.65	50%	2.43
TFN RO — conventional	15.3	55	59.4	19.93	80%	0.43	50%	2.58
TFN RO — conventional	17.0	45	53.4	20.20	78%	1.18	60%	2.49
TFN RO — conventional	17.0	50	57.9	21.28	81%	0.69	70%	2.54
TFN RO — hybrid 1	12.0	40	46.1	12.72	74%	0.99	55%	2.24
TFN RO — hybrid 1	12.0	45	49.1	13.14	77%	0.62	50%	2.24
TFN RO — hybrid 1	12.0	50	53.1	13.88	78%	0.40	50%	2.34
TFN RO — hybrid 1	12.0	55	58.1	15.19	78%	0.25	40%	2.53
TFN RO — hybrid 1	15.3	45	52.0	18.02	77%	1.20	55%	2.43
TFN RO — hybrid 1	15.3	50	55.2	18.79	77%	0.75	60%	2.46
TFN RO — hybrid 1	15.3	55	59.9	19.68	80%	0.49	45%	2.55
TFN RO — hybrid 1	18.7	50	59.0	23.99	77%	1.39	55%	2.61
TFN RO — hybrid 1	18.7	55	61.8	25.27	78%	0.77	60%	2.68
TFN RO — hybrid 2	12.0	40	46.2	11.70	81%	0.70	55%	2.17
TFN RO — hybrid 2	12.0	45	49.2	12.19	83%	0.42	50%	2.20
TFN RO — hybrid 2	12.0	50	53.6	13.19	82%	0.28	50%	2.36
TFN RO — hybrid 2	12.0	55	57.7	13.83	85%	0.18	40%	2.46
TFN RO — hybrid 2	15.3	45	51.8	16.66	83%	0.73	55%	2.35
TFN RO — hybrid 2	15.3	50	55.2	17.33	84%	0.54	60%	2.41
TFN RO — hybrid 2	15.3	55	60.8	18.58	86%	0.36	45%	2.58
TFN RO — hybrid 2	18.7	50	58.0	22.22	83%	0.89	55%	2.57
TFN RO — hybrid 2	18.7	55	62.5	23.94	83%	0.58	60%	2.74

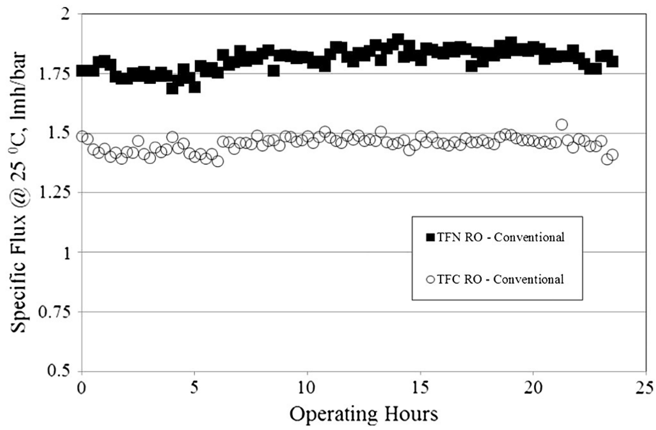

Fig. 3. Comparison of temperature corrected specific flux between TFN and TFC RO membranes in the conventional configuration. The 1st pass RO system was operated at a flux of 15.3 lmh and a feed water recovery of 50%.

for both conventional and hybrid configurations. Due to the lower concentrate flow rate at this high recovery condition, the efficiency of the ERD booster pump was the lowest (40%) at this operating condition.

3.3. Energy consumption of TFN RO membranes

Experiments were performed at varying operating conditions using the TFN RO membranes in conventional and hybrid configurations. Experimental SEC for TFN RO membranes is shown in Table 5. For an operational flux of 12.0 lmh, the SEC for TFN RO membranes ranged between 2.19 kWh/m^3 and 2.53 kWh/m^3. With an increase in feed water recovery, the power used by the high pressure pump increased due to a higher feed pressure requirement to maintain a constant flux. However, the power requirement for the ERD booster pump decreased with an increase in feed water recovery due to the lower concentrate flow generated at higher feed water recoveries. In order to determine the difference in permeability, the specific flux was calculated for the TFN and TFC RO membranes in the conventional configuration. A comparison of the specific flux is shown in Fig. 3. The average specific fluxes for TFN and TFC RO membranes were 1.72 lmh/bar and 1.48 lmh/bar, respectively. This showed a 14% higher specific flux when compared to the TFC RO membranes utilized in this study.

A correlation between experimental and calculated SEC for the TFN RO membranes is shown in Fig. 4. The calculated SEC values were lower when compared to the experimental SEC values. The efficiency of the high pressure and ERD booster pump is shown in Table 5 for various operating conditions with TFN RO membranes. The high pressure pump operated at its highest efficiency of 88% at a flux of 15.3 lmh and a 1st pass feed water recovery of 45% for the conventional

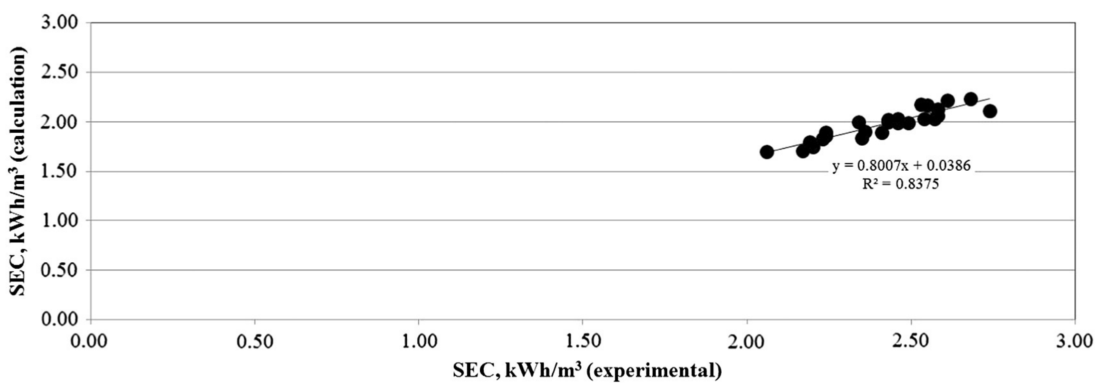

Fig. 4. Comparison of experimental and calculated specific energy consumption for TFN RO membranes.

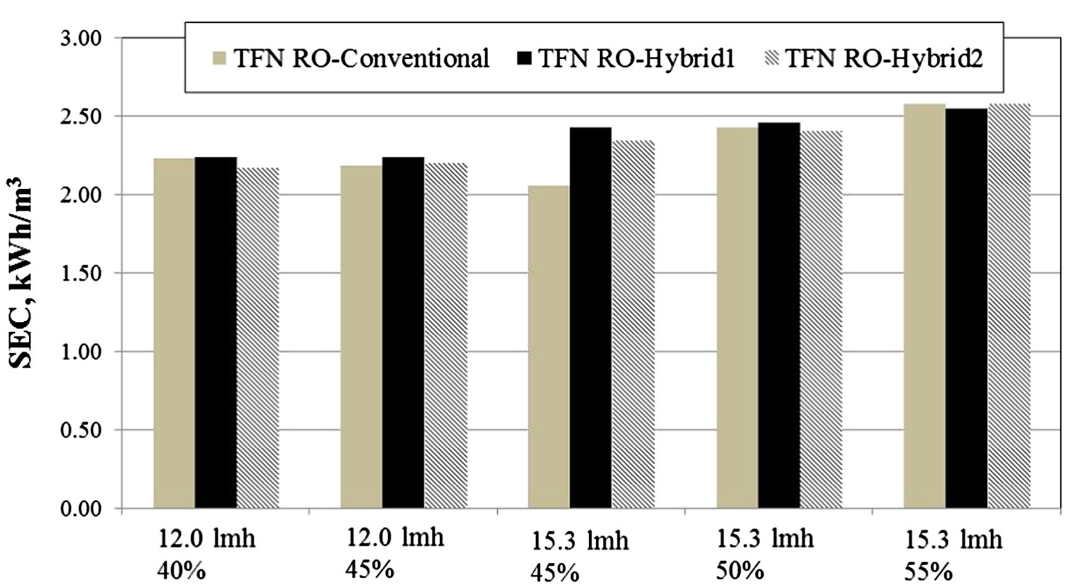

Fig. 5. Comparison of SEC for TFN membranes in the conventional and hybrid configurations at varying flux and recovery conditions.

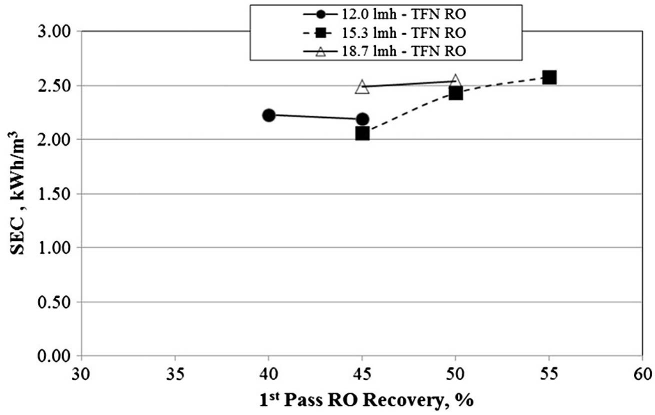

Fig. 6. Comparison of SEC for TFN RO membranes at varying recoveries operated in the conventional configuration.

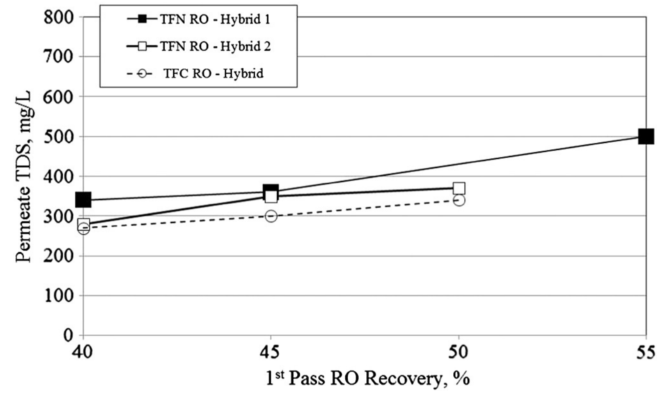

Fig. 9. Permeate TDS concentration for model membranes operated in the hybrid configuration at an operational flux of 12.0 lmh.

configuration. However, the high pressure pump efficiency was highest (86%) at a flux of 15.3 lmh and a 1st pass recovery of 55% for the hybrid configuration. This efficiency range is typical for axial piston pumps used for high pressure applications. The efficiency of the ERD booster pump ranged between 50% and 70%, depending on the flow and output pressure requirements. Higher measured SEC when compared to the calculated SEC could be as a result of additional loss in efficiency of the pumps, such as heat loss and lack of periodic maintenance resulting in lower working efficiency and higher energy consumption.

A comparison of TFN RO membrane SEC for operation in conventional and hybrid configurations is shown in Fig. 5. Utilization of a hybrid design results in better flux distribution within the pressure vessel and minimizes the lead element flux. In general, the SEC was not substantially different for operation in the conventional and hybrid configurations. Similarly, the feed pressure was not substantially different for operation of SWRO elements in conventional and hybrid configurations at similar fluxes and recoveries.

A comparison of SEC for TFN RO membranes at varying fluxes and recoveries is shown in Figs. 6, 7 and 8 for conventional, hybrid 1 and

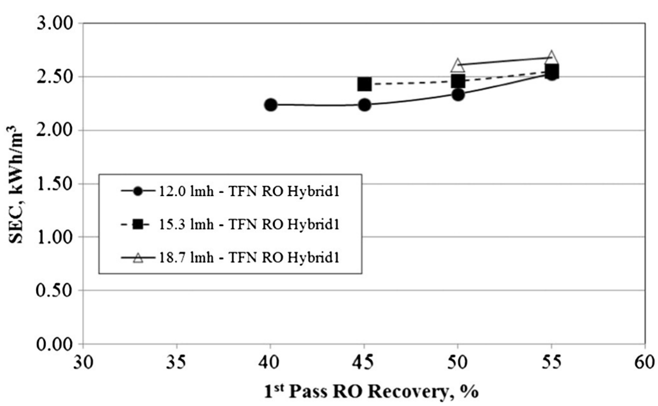

Fig. 7. Comparison of SEC for TFN RO membranes at varying recoveries operated in the hybrid 1 configuration.

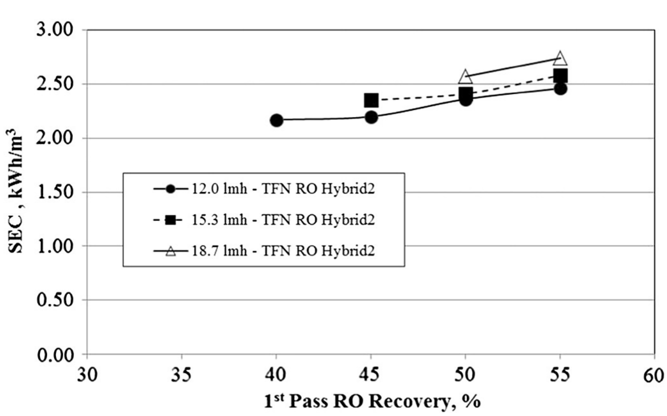

Fig. 8. Comparison of SEC for TFN RO membranes at varying recoveries operated in the hybrid 2 configuration.

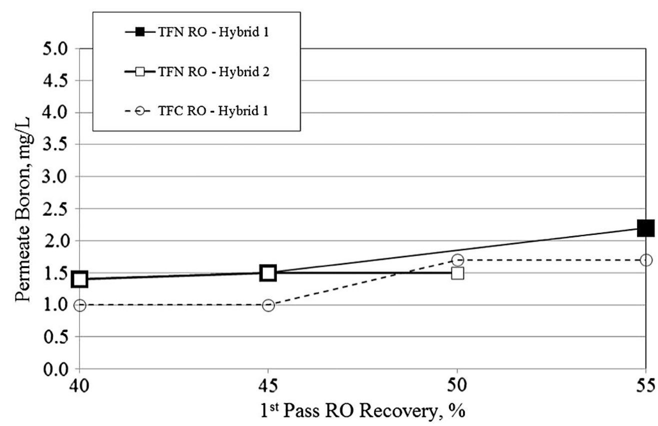

Fig. 10. Permeate boron concentration for model membranes operated in the hybrid configuration at an operational flux of 12.0 lmh.

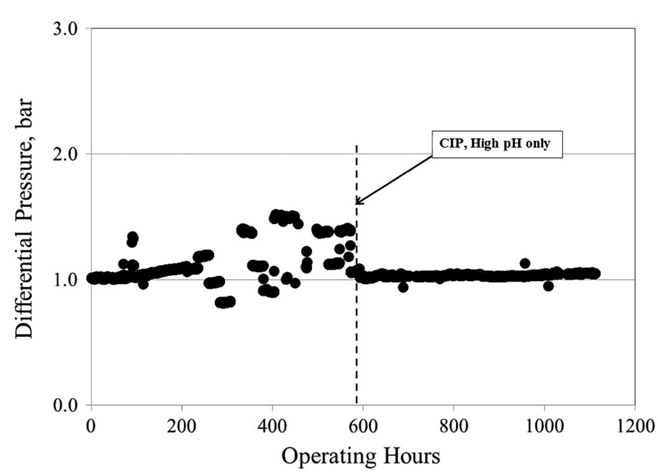

Fig. 11. Differential pressure profile for TFN RO membranes operated in the hybrid configuration at a flux of 15.3 lmh and a 1st pass recovery of 50%.

Table 6
Presence of spectral bands associated with FT-IR analysis of TFN RO membranes surface after pilot scale testing.

Peaks	Yes	Weak
C–H		X
C–N	X	
N–H	X	
C–C	X	
C–C	X	
H–C–OH	X	
N–H–C═O	X	
N–C═O	X	
C–O–C	X	

hybrid 2 configurations, respectively. For most conditions, the SEC increased with an increase in feed water recovery due to higher feed pressure requirements. Similarly, an increase in flux resulted in a higher SEC. However, the SEC was not substantially different for operation in the conventional and hybrid configurations. For example, at a recovery of 50% and flux of 15.3 lmh, the SEC was 2.50 kWh/m^3 for both conventional and hybrid configurations.

3.4. Rejection, fouling and cleaning studies with TFN RO membranes

Permeate TDS and boron concentrations for model membranes at 12.0 lmh are presented in Figs. 9 and 10, respectively. Based on the measured concentration of TDS and boron in the permeate at varying recovery conditions, the TFN RO membranes utilized in this study exhibited lower rejection than TFC RO membranes. As the feed water recovery increased, TDS and boron concentrations in the permeate increased. An increase in recovery results in a higher concentration factor across the membrane surface, resulting in higher diffusion of solute (salt) molecules through the membrane surface. This in turn causes higher TDS and boron concentrations at higher recovery levels.

Differential pressure across the 1st pass RO system with TFN RO membranes in hybrid 1 configuration is shown in Fig. 11. The differential pressure steadily increased and after the differential pressure rose to approximately 1.6 bar, the system was cleaned-in-place (CIP) after 600 h of operation using sodium hydroxide at pH of 11.0. After CIP, the differential pressure decreased to the initial value of 1 bar and remained constant for the reminder of the study. The increase in differential pressure was probably due to an increase in TOC concentration in the feed seawater. The TOC concentration doubled during this period which resulted in organic fouling of the membranes. It should be noted that the TFN and TFC RO membranes were not evaluated in parallel. During operation of the TFC RO membranes, there were no substantial changes in the feed water quality and the TOC concentrations remained stable. Thus, fouling events did not occur during evaluation of the TFC RO membranes. The fouling and cleaning efficacy of the TFN RO membranes are shown only to represent the nature of fouling and efficacy of chemical cleaning and not as a direct comparison to TFC RO membranes.

In order to determine the nature of the foulant layer deposited on the TFN RO membrane surface, FT-IR spectroscopy was performed. The FT-IR spectra were utilized to identify organic functional groups on the fouled membrane surface. A summary of the organic functional bands identified during spectroscopic analysis is shown in Table 6. Based on the spectral analysis, the presence of protein-like and carbohydrate-like materials deposited on the membrane surface was evident and confirmed organic fouling. From the SEM analysis (not shown), the foulant layer was not uniformly deposited on the membrane surface and appeared to be in small patches.

Table 7
Flow, pressure and water quality at various locations along the treatment train depicted in Fig. 1. The 1st pass was operated at a flux of 15.3 lmh and a feed water recovery of 50%. The 2nd pass was operated at a flux of 27.5 lmh and a feed water recovery of 90%.

	A	B	C	D	E
Flow, m^3/h	15.9	3.3	4.7	4.2	7.5
TFC RO — hybrid configuration					
TDS, mg/L	35,000	82	394	10	41
Boron, mg/L	4.50	0.50	1.90	0.21	0.34
Pressure, bar	61.6	1.0	10.3	1.0	1.0
TFN RO — hybrid 1 configuration					
TDS, mg/L	35,000	80	510	13	42
Boron, mg/L	4.50	0.50	2.20	0.24	0.37
Pressure, bar	57.7	1.0	10.7	1.0	1.0
TFN RO — hybrid 2 configuration					
TDS, mg/L	35,000	80	470	12	42
Boron, mg/L	4.50	0.50	2.30	0.25	0.38
Pressure, bar	55.2	1.0	10.5	1.0	1.0

3.5. SEC of entire RO system

Power consumption for all the pumps utilized in the 1st and 2nd pass RO systems was measured to determine the total energy consumption of the RO system. A schematic of pump locations is provided in Fig. 1. Permeate from the tail elements in the 1st RO pass was utilized as feed to the 2nd pass of the RO system. A comparison of the feed pressure and permeate water quality for the entire RO system using TFC and TFN RO membranes is provided in Table 7. Power consumption for the four pumps and total SEC for the RO system is shown in Table 8. The power consumption of pumps in the 1st pass RO system was empirically determined whereas that for the 2nd pass feed pump was calculated. Due to inferior permeate water quality (based on TDS) produced by TFN RO tail elements, a higher feed pressure was required by the 2nd pass RO system, resulting in higher power consumption by the 2nd pass feed pump. The total SEC of the RO system (1st pass and 2nd pass) with TFN RO membranes in the hybrid 1 configuration and hybrid 2 configuration in the 1st pass were 3.45 kWh/m^3 and 3.24 kWh/m^3, respectively. The SEC was 3.60 kWh/m^3 with TFC RO membranes in the 1st pass. Thus, for achieving similar blended permeate water qualities (boron < 0.5 mg/L and TDS < 350 mg/L) after the 2nd pass RO system, energy savings using TFN RO hybrid 1 and hybrid 2 configuration were approximately 4% and 10%, respectively.

4. Conclusions

Application of TFN RO membranes for seawater desalination could potentially result in up to 10% savings in energy consumption. The SEC for TFN RO membranes at various operating conditions was evaluated for

Table 8
Power consumption of individual pumps and total SEC for the entire RO system employed in study. The 1st pass was operated at a flux of 15.3 lmh and a feed water recovery of 50%. The 2nd pass was operated at a flux of 27.5 lmh and a feed water recovery of 90%.

1st pass membrane configuration	Pump power, kW				Total power, kW	Total SEC, kWh/m^3
	Pump 1	Pump 2	Pump 3	Pump 4		
TFC RO — hybrid configuration	4.7	20.2	0.5	1.5	26.9	3.60
TFN RO — hybrid 1 configuration	4.7	18.8	0.7	1.6	25.8	3.45
TFN RO — hybrid 2 configuration	4.7	17.3	0.6	1.6	24.2	3.24

seawater desalination and compared to TFC RO membranes. Utilization of TFN RO membranes resulted in a lower feed pressure and lower SEC when compared to TFC RO membranes. For an operational flux of 12.0 lmh, the SEC for TFC RO membranes ranged between 2.28 kWh/m^3 and 2.62 kWh/m^3 for the 1st pass RO system. For the same operational flux, the SEC for TFN RO membranes ranged between 2.19 kWh/m^3 and 2.53 kWh/m^3 for the 1st pass RO system. Selection of TFN RO membranes over TFC RO membranes also requires a careful consideration of life cycle costs. When the TFN RO membrane element cost is higher, capital costs will be higher. However, life cycle costs of the plant could potentially be lower due to savings in energy costs over the plant operational life.

Acknowledgments

The results from this paper were based on a project funded by the WateReuse Research Foundation (WRRF #11-04) and the authors would like to thank the Project Manager, Kristan Cwalina. The authors would also like to thank Shivaji Deshmukh, Diane Gatza and Frank Fuchs from the West Basin Municipal Water District for providing the pilot test site. Thanks to Robert Burk, David Kim-Hak and Mike Dixon from NanoH_2O, LLC for providing membrane elements during the study. The project team would like to acknowledge operational support provided by Silvana Ghui and Gerry Filteau from Separation Processes Inc. and Kevin Tirado from United Water.

References

[1] Q. Schiermeier, Water: purification with a pinch of salt, Nature 452 (2008) 260–261.
[2] L.G. Greenlee, D.F. Lawler, B.D. Freeman, B. Marrot, P. Moulin, Reverse osmosis desalination: water sources, technology, and today's challenges, Water Res. 43 (2009) 2317–2348.
[3] S. Loeb, S. Sourirajan, Seawater demineralization by means of an osmotic membrane, Adv. Chem. Ser. 38 (1963) 117–132.
[4] A. Subramani, M. Badruzzaman, J. Oppenheimer, J.G. Jacangelo, Energy minimization strategies and renewable energy utilization for desalination: a review, Water Res. 45 (2011) 1907–1920.
[5] R.G. Raluy, L. Serra, J. Uche, Life cycle assessment of desalination technologies integrated with renewable energies, Desalination 183 (2005) 81–93.
[6] D.R. Paul, Reformulation of the solution–diffusion theory of reverse osmosis, J. Membr. Sci. 241 (2004) 371–386.
[7] M. Wilf, C. Bartels, Optimization of seawater RO systems design, Desalination 173 (2005) 1–12.
[8] R. Stover, Seawater reverse osmosis with isobaric energy recovery devices, Desalination 203 (2007) 168–175.
[9] M. Elimelech, W.A. Phillip, The future of seawater desalination: energy, technology, and the environment, Science 333 (2011) 712–717.
[10] T. Seacord, J. MacHarg, S. Coker, Affordable desalination collaboration 2005 results, Proceedings of the American Membrane Technology Association Conference in Stuart, FL, USA, July 2006.
[11] R. Semiat, Energy issues in desalination processes, Environ. Sci. Technol. 42 (2008) 8193–8201.
[12] R.R. Nair, H.A. Wu, P.N. Jayaram, I.V. Grigorieva, A.K. Geim, Umimpeded permeation of water through helium-leak-tight graphese-based membranes, Science 27 (2012) 442–444.
[13] S.C. O'Hern, M.S.H. Boutilier, J.C. Idrobo, Y. Song, J. Kong, T. Laoui, M. Atieh, R. Karnik, Selective ionic transport through tunable subnanometer pores in single-layer graphene membranes, Nano Lett. 14 (2014) 1234–1241.
[14] R.K. Joshi, P. Carbone, F.C. Wang, V.G. Kravets, Y. Su, I.V. Grigorieva, H.A. Wu, A.K. Geim, R.R. Nair, Precise and ultrafast molecular sieving through graphene oxide membranes, Science 343 (2014) 752–754.
[15] D.S. Sholl, J.K. Johnson, Making high-flux membranes with carbon nanotubes, Science 312 (2006) 1003–1004.
[16] J.K. Holt, H.G. Park, Y.M. Wang, M. Stadermann, A.B. Artyukhin, C.P. Grigoropoulos, A. Noy, O. Bakajin, Fass mass transport through sub-2-nanometer carbon nanotubes, Science 312 (2006) 1034–1037.
[17] P.S. Goh, A.F. Ismail, B.C. Ng, Carbon nanotubes for desalination: performance evaluation and current hurdles, Desalination 308 (2013) 2–14.
[18] C.H. Ahn, Y. Baek, C. Lee, S.O. Kim, S. Kim, S. Lee, S. Kim, S.S. Bae, J. Park, J. Yoon, Carbon nanotube-based membranes: fabrication and application to desalination, J. Ind. Eng. Chem. 18 (2012) 1551–1559.
[19] M. Kumar, M. Grzelowski, J. Zilles, M. Clark, W. Meier, Highly permeable polymeric membranes based on the incorporation of the functional water channel protein Aquaporin Z, Proc. Natl. Acad. Sci. U. S. A. 104 (2007) 20719–20724.
[20] F.Q. Zhu, E. Tajkhorshid, K. Schulten, Theory and simulation of water permeation in aquaporin-1, Biophys. J. 86 (2004) 50–57.
[21] J.E. Cadotte, R.J. Petersen, R.E. Larson, E.E. Erickson, A new thin-film composite seawater reverse osmosis membrane, Desalination 32 (1980) 25–31.
[22] C.J. Kurth, R.L. Burk, J. Green, Utilizing nanotechnology to enhance RO membrane performance for seawater desalination, International Desalination Association (IDA) World Congress, Perth, Western Australia, September 4–9, 2011, 2011.
[23] M.G. Buonomenna, Nano-enhanced reverse osmosis membranes, Desalination 314 (2013) 73–88.
[24] B.H. Jeong, E.M.V. Hoek, Y. Yan, A. Subramani, X. Huang, G. Hurwitz, A.K. Ghosh, A. Jawor, Interfacial polymerization of thin film nanocomposites: a new concept for reverse osmosis membranes, J. Membr. Sci. 294 (2007) 1–7.
[25] M.M. Pendergast, A.K. Ghosh, E.M.V. Hoek, Separation performance and interfacial properties of nanocomposite reverse osmosis membranes, Desalination 308 (2013) 180–185.
[26] C.J. Kurth, J.A. Koehler, M. Zhou, B.A. Holmberg, R.L. Burk, Reverse osmosis membranes, Patent US 8177978 B2, Available at http://www.google.com/patents/US8177978 , Last accessed: April 8, 2014.
[27] C.J. Kurth, J.A. Koehler, M. Zhou, B.A. Holmberg, R.L. Burk, Hybrid nanoparticle TFC membranes, Patent US 8603340 B2, Available at http://www.google.com/patents/US8603340 , Last accessed: April 8, 2014.
[28] B. Hofs, R. Schurer, D.J.H. Harmsen, C. Ceccarelli, E.F. Beerendonk, E.R. Cornelissen, Characterization and performance of a commercial thin film nanocomposite seawater reverse osmosis membrane and comparison with a thin film composite, J. Membr. Sci. 446 (2013) 68–78.
[29] Qfx SW400ES, Specification Sheet, Available at http://www.nanoh2o.com/products/qfx-sw-400-es (Last accessed: April 8, 2014).
[30] Qfx SW400R, Specification Sheet, Available at http://www.nanoh2o.com/products/qfx-sw-400-r (Last accessed: April 8, 2014).
[31] SW30ULE-400i, Specification Sheet, Available at http://www.dowwaterandprocess.com/en/products/f/filmtec_sw30ule_400i (Last accessed: April 8, 2014).
[32] SW30XLE-400i, Specification Sheet, Available at http://www.dowwaterandprocess.com/en/products/f/filmtec_sw30xle_400i (Last accessed: April 8, 2014).
[33] Reverse Osmosis (RO) Technical Manual, http://www.dowwaterandprocess.com/en/resources/reverse-osmosis-technical-manual Dow Filmtec Corporation, 2014. (Last accessed: June 30, 2014).
[34] R.P. Schneider, L.M. Ferreira, P. Binder, J.R. Ramos, Analysis of foulant layer in all elements of an RO train, J. Membr. Sci. 261 (2005) 152–162.